Article

Noise suppression of high-speed cavity treated with leading and trailing edge spoilers

Dongping Yin, Yang Liu*, **Dangguo Yang, Yong Luo, Fangqi Zhou, Bin Dong***, **Ronghui Ning, Chunhui Yan**

China Aerodynamics Research and Development Center, Mianyang 621000, China

* Corresponding author: Yang Liu, ly2020_article@126.com, ly22article@cardc.cn; Bin Dong, nudt18214@163.com, dongbin@cardc.cn

Abstract: High-speed cavity flow and the induced noise have been continuously investigated in the aerospace industry. They may not only influence the performance of instruments inside the cavity, but also cause fatigue damage to the structures, which threaten the safety of aircraft. Therefore, cavity noise suppression is practically important. In this work, the leading edge sawtooth, the leading edge cylinder, and the trailing edge contouring are employed to suppress high-speed cavity noise at Mach numbers of 2.0, 2.5, 3.0, 3.5, and 4.0. Wind tunnel tests were performed to study the influence of the control parameters associated with these suppression methods. The results show that the leading edge sawtooth and cylinder are able to effectively suppress cavity noise at Ma = 2.0, 2.5, but prove ineffective at Ma = 3.0, 3.5, and 4.0, suggesting that the critical Mach number locates between 2.5 and 3.0. Above the critical Mach number, cavity noise would increase. In comparison, the noise suppression effect of the trailing edge contouring is relatively minor, and it shows a monotone decreasing trend as Mach number increases from 2.0 to 4.0.

Keywords: high-speed cavity; noise suppression; leading edge sawtooth; leading edge cylinder; trailing edge contouring

1. Introduction

Cavity noise is prevalent in the aerospace industry, such as the internally buried bomb bay of advanced fighter aircraft [1] and the landing gear bay of airplane [2]. Given that certain aerodynamic and geometrical shape conditions are satisfied, when high-speed air flow across the cavity, severe pressure pulses would be generated with high intensity noise, which not only deteriorates the cavity flow field, but also poses threats to the structural safety of the equipment inside the cavity and the cavity itself. Therefore, cavity noise suppression is widely pursued [3,4]. Among various methods to suppress cavity noise, spoiler control of the leading edge of cavity is a simple and effective method. Stanek et al. [5] studied the effects of interference flow devices on the flow and noise inside the cavity, including leading edge sawtooth, leading edge cylinder and cylinder surrounded by thin wire. Schmit et al. [6,7] used high-speed photography technique to study the effect of leading edge plate, leading edge cylinder and sawtooth on cavity flow and noise under supersonic conditions. They found that the leading edge spoiler device could cut down the flow into the cavity by lifting the position of the shear layer, and thus suppressing the high intensity cavity noise. Thangamani et al. [8,9] investigated the suppression effect of leading edge sawtooth on cavity noise, and pointed out that the leading edge sawtooth was able to change the three-dimensional structural characteristics above the cavity and therefore damaged its continuity. Panichar and Raman et al. [10] studied the effect of leading edge

cylinder on cavity noise and self-sustaining oscillation, and their results showed out that the leading edge cylinder could suppress cavity noise within a large speed range. Dudley and Ukeiley et al. [11,12] found that the leading edge cylinder could make the shear layer deflect to the outside of the cavity, and thus lift the position of the shear layer and increased its thickness and stability, which could effectively decrease the impact caused by collision with the aft wall of the cavity. Yang and Wu et al. [13] studied the cavity noise suppression through added leading edge sawtooth, blowing-suction device and rear wall fillet to the cavity in sub transonic wind tunnel tests.

In 2020, Ananthan [14–16] researched the impact of porous materials on the trailing edge of an airfoil. Their findings revealed that the cross-surface pressure coherence of the coherent vortex was significantly disrupted, resulting in a reduction in the mean convection velocity. In 2022, the noise reduction capabilities of locally applied shallow depression surfaces at the trailing edge were further explored. The application of shallow depressions was found to disrupt cross-coherence and decrease the vortical convection velocity, particularly in the middle and low frequency bands. In 2023, the trailing edge noise reduction potential of locally applied shallow depression surfaces was scrutinized. Analysis of the trailing edge noise revealed a decrease in flow velocity within the trailing edge channel, which positively contributed to reducing noise levels. During the same year, Ananthan [17] also investigated the utilization of bionic fish fins as a method to mitigate tail-edge noise. The observed boundary layer turbulence statistics and surface pressure fluctuation spectral density spectra were in close alignment with the experimental data. Early researchers attempted to analyze the mechanism of cavity flow-induced noise through wind tunnel noise spectra and Schlieren images, aiming to establish a predictive model for cavity flow-induced noise spectra [18]. At the leading edge of the cavity, small disturbances within the shear layer trigger Kelvin-Helmholtz instability, resulting in vortex shedding at the leading edge and their subsequent propagation toward the rear edge of the cavity. As these unstable vortices propagate, the free flow above the cavity continuously feed them with energy, amplifying the disturbances through convective processes. When the unstable vortices strike the back edge of the cavity, they scattered sound waves upstream. The sound waves that travel toward the leading edge of the cavity were reflected and then propagated downstream. When ascending and descending sound waves aligned under specific phase conditions, they resonated, generating a pure tone. Additionally, as the acoustic waves disturbed the front edge of the cavity, the shear layer's disturbance intensified, creating a self-sustaining system with positive feedback within the entire cavity. This feedback loop was further influenced by the structural response of the cavity wall. Plumbee et al. [19] developed an acoustic impedance model by treating the pulsating pressure within the cavity as an excitation source. The spectral response of the noise was dictated by the model's transfer function, while the noise intensity was determined by the impedance. Hankey [20] employed the MacCormack scheme to solve two-dimensional compressible Navier-Stokes equations for the flows of the cavity with a length-to-depth ratio of 2.25, an incoming Mach number of 1.5, and a Reynolds number of 2.6×10^7. This marked the first time a numerical solution for the cavity flow field was obtained. Current research on cavities primarily focuses on subsonic and transonic flow. The effect of

high Mach number on flow [21, 22] and the study of high-speed cavity [23–25] are mainly rely on numerical simulations. For instance, Chen et al. [26] conducted nonlinear numerical simulations to investigate aerodynamic noise control in supersonic aircraft cavities. Notably, only limited literatures [27,28] have reported the use of wind tunnel tests for high-speed cavity.

With C201 cavity standard model [29–32] as the research subject, this article utilized wind tunnel test to measure the dynamic pressure within the cavity. By comparing the noise Sound Pressure Level distribution within the cavity under various control parameters, the effect and influence principles of leading edge sawtooth, cylinder and trailing edge contouring on cavity flowing noise under the supersonic conditions were analyzed, which provided theoretical foundation and method reference for establishment of control strategies with engineering use value.

2. Test setup and data processing

2.1. Wind tunnel and measurement system

The wind tunnel tests were conducted in China Aerodynamics Research and Development Center (CARDC). The wind tunnel was of an intermittent and half-return-flow type, with a test section measuring 600 mm high, 600 mm wide, and 2500 mm long. It was capable of operating at Mach numbers ranging from 0.3 to 4.5. The range of total pressure was 95 kPa to 720 kPa, and the range of Reynolds numbers (Re) was $(0.33{\sim}8.9) \times 10^7$ per unit length. The wall of the test section of the wind tunnel could be changed according to type of test, and the four walls were solid walls during the supersonic test.

The piezoresistive pressure sensors with a range of 50 psi, a sampling frequency of 50 kHz and a sampling time of 10 s were used to measure the fluctuating pressure inside the cavity.

2.2. Test model and test conditions

The test model has a total length of 514 mm and a total width of 320 mm, as shown in **Figure 1a**. There are 9 measuring points of fluctuating pressure on the axle wire at the bottom of the cavity. Both the inner wall of the leading edge and trailing edge have 1 measuring point. The aperture of those points is 1.7 mm. The position of pressure sensors in the model is shown in **Figure 1b**, in which x/L is the ratio between streamwise coordinates and cavity length. The cavity has a length (L) of 200 mm, a depth (D) of 33.3 mm, and a width (W) of 66.7 mm, resulting in a length-to-depth ratio (L/D) of 6 and a width-to-depth ratio (W/D) of 2. In the test, the attack angle α is 0°, and the incoming flow Mach number are 2.0, 2.5, 3.0, 3.5 and 4.0 respectively, and the corresponding Re are 2.388×10^7, 2.644×10^7, 2.827×10^7, 3.244×10^7 and 2.9×10^7 per unit length, respectively.
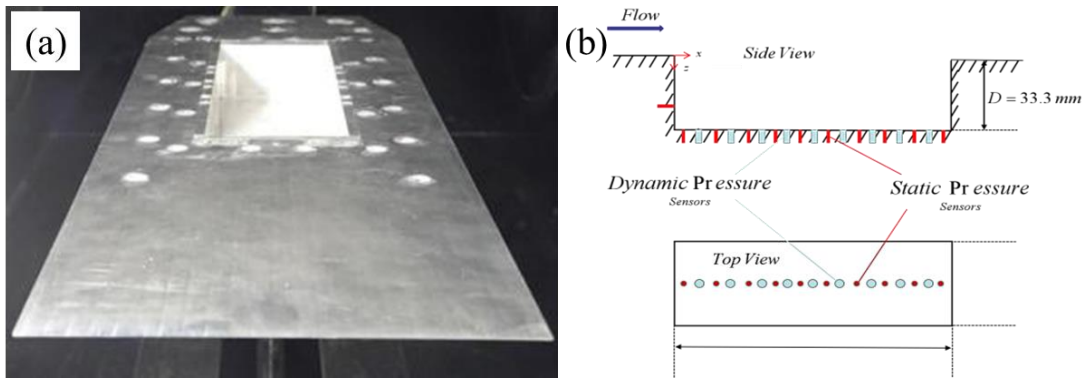
Figure 1. Test state of the model. **(a)** photograph of the test model; **(b)** position of pressure sensors in the model.

As the model is to finish several tests of control methods like leading edge spoiler and trailing edge contouring, parts of the control devices need to be installed through the screw hole. The smooth plate of 200 mm length is between the slot at the leading edge of the cavity used to install the leading edge spoiler and the leading edge of model, and they are mainly used to simulate and control the thickness of the incoming flow boundary layer.

The geometrical shape of leading edge sawtooth is characterized by the total length H, bottom height h, sawtooth height h^*, and the sawtooth angle is $60°$ (as shown in **Figure 2a**). In comparison, the geometrical shape of leading edge cylinder is determined by cylinder diameter R, support column height e, and the length of the cylinder is 68 mm (as shown in **Figure 2b**). The geometrical shape of the trailing edge contouring is determined by θ (as shown in **Figure 2c**).
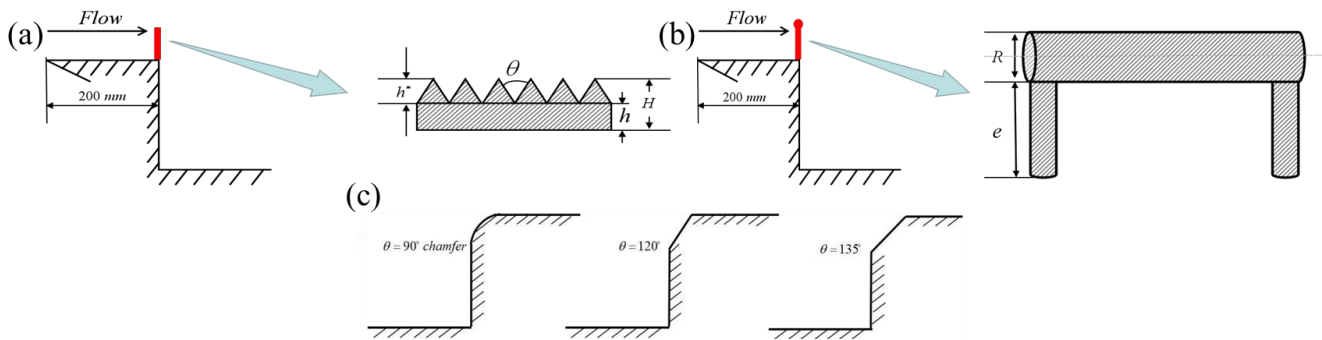

Figure 2. Schematic diagrams for **(a)** the leading edge sawtooth spoiler; **(b)** the leading edge cylinder; **(c)** the trailing edge contouring.

2.3. Data processing

Sound Pressure Level (*SPL*) mainly reflects the strong and weak characteristics of pressure pulse at the measuring points, and Sound Pressure Frequency Spectra (*SPFS*) reflects the frequency domain characteristics of pressure pulse power at the measuring points. The domain signals collected through the fluctuating pressure sensors include DC and AC components. When the DC ones eliminated through filtering processing, the AC ones *P(t)* would be remained, and the calculation formula of its root mean square (p_{rms}) is as follows:

$$p_{rms} = \lim_{T \to \infty} \sqrt{\frac{1}{T} \int_{0}^{T} p^2(t)dt} \tag{1}$$

In the Equation (1), *T* is the length of the sample. Thus, the *SPL* of domain sample while obtaining fluctuating pressure is as follows:

$$SPL = 20\lg \frac{p_{rms}}{p_{ref}} \tag{2}$$

In the Equation (2), $p_{ref} = 2.0 \times 10^{-5}$ Pa is the reference pressure. The *SPL* of samples reflects the intensity of pressure pulse in the flow field at the measuring points, which could effectively describe the distribution of noise inside the cavity.

The Pressure Spectral Density (*PSD*) of fluctuation pulse samples were adopted, then the *SPFS* of samples could be obtained through the Equation (3), thus spectral analysis of noise inside the cavity could be carried out.

$$SPFS = 10\log \frac{PSD}{p_{ref}^2} \tag{3}$$

3. Results and discussion

3.1. Numerical schlieren

An analysis is undertaken of the transient flow field derives from unsteady numerical simulations, specifically in conditions where the Mach number is set at 2 and 3, with an aspect ratio of L/D = 6. The numerical simulation is commenced in accordance with the parameters establish in prior literature. Additionally, the condition of the dimensionless calculation area positioned above the cavity is determined based on the flow reference values obtained from wind tunnel tests.

The increasingly intricate pulsatile structure of the cavity at higher Mach numbers is clearly depicted in **Figure 3**. Specifically, a small impact structure emerges within the shear layer at the leading edge of the cavity. However, as the shear layer moves downstream, this small shock structure dissipates rapidly, indicating that the local convective Mach number remains below 0.7 [33], preventing the shock structure from being sustained. The small shock structure manages to traverse nearly half the distance to the downstream convective cavity at Ma = 3, as shown in **Figure 3b**. This observation highlights that the convective velocity of the shear layer within the downstream cavity also rises as Ma increases. When Ma = 2, the shear layer within the cavity rapidly destabilizes due to downstream convection, as shown in **Figure 3a**. Conversely, the shear layer destabilizes without significant disturbance amplification, revealing a regular small shock structure at the leading edge of the cavity when Ma = 3. These findings indicate that the stability of the compressible shear layer improves as the Mach number increases.
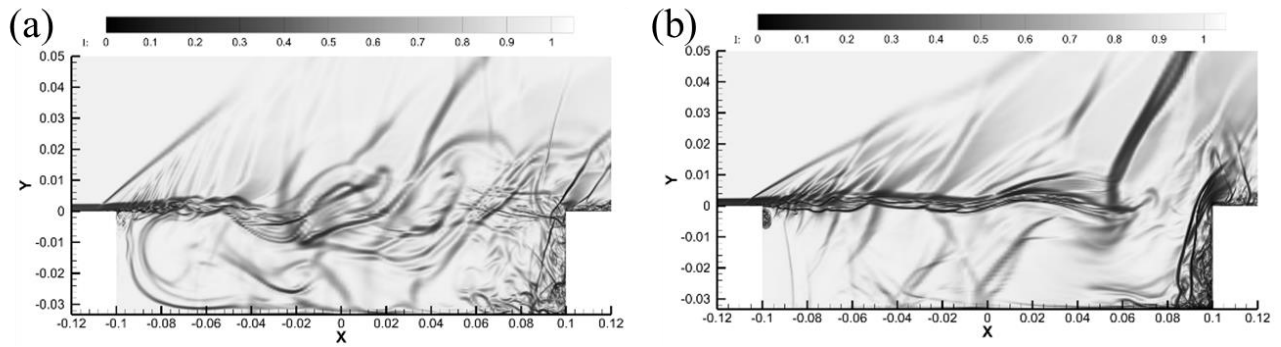
Figure 3. Numerical schlieren of a cavity. **(a)** Ma = 2, L/D = 6; **(b)** Ma = 3, L/D = 6.

3.2. Suppression effect of leading edge sawtooth on high-speed cavity noise

Through comparing the *SPL* distribution curves on the centerline of the inner wall of the cavity under leading edge sawtooth control of various dimension parameters, the influence of leading edge sawtooth on cavity noise could be analyzed, and concrete dimensions of the leading edge sawtooth are as shown in **Figure 4**.
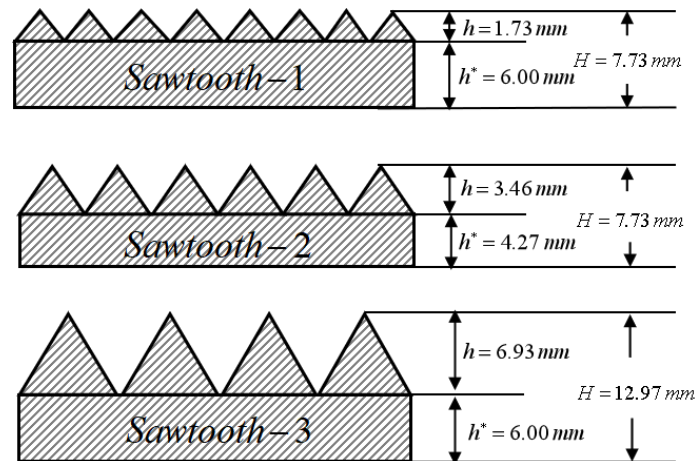

Figure 4. Leading edge sawtooth of various parameters.

The *SPL* distribution of various measuring points within the cavity under leading edge sawtooth of various parameters in all Mach numbers are shown in **Figure 5**. In the cavity $x/L < 0.5$ region, along with the streamwise position of the centerline within the cavity, the *SPL* show a decreasing trend, followed by an increasing one, and the *SPL* within the cavity is the smallest in the cavity $x/L = 0.2$. In the cavity $x/L > 0.5$ region, the *SPL* shows an increasing-decreasing-increasing trend along with the streamwise position of the centerline within the cavity, and the maximum *SPL* within the cavity appears at the $x/L = 1.0$ at the aft wall of the cavity. Some studies [34,35] have shown that the change in the thickness of the leading edge would lead to slight changes in the incidence angle between the air flow and the front wall of the cavity. The leading edge straight plate could greatly raise the position of the shear layer, which would make the downstream impact area of the cavity move backward, thus weakening the flow rate and intensity of the fluid entering the cavity. At the same time, it could reduce the static pressure in the cavity and reduce the intensity and range of

the return flow, which has a significant suppression effect on the noise in the cavity. As leading edge sawtooth could also increase the location of the shear layer and reduce intensity of the return flow within the cavity, it has similar suppression effect on noise within the cavity. It can be seen from the *SPL* curves (**Figure 5**) that when Ma = 2.0 and 2.5, the noise suppression effect of *Sawtooth*-2 is the worst, while that of *Sawtooth*-1 and *Sawtooth*-3 is similar. But the increase of leading edge sawtooth height would increase the projected area in the normal direction of the incoming flow, causing increase of resistance near the cavity and thus would influence the aerodynamic performance and flight performance of the craft. Therefore, taking both the noise suppression effect and aerodynamic performance into consideration, the comprehensive performance of *Sawtooth*-1 is better than others. The decrease of SPL at the cavity x/L = 0.8 under the control of *Sawtooth*-1 could reach 7.18 dB when Ma = 2.0, and when Ma = 2.5, the control effect declines and the decrease of *SPL* at the cavity x/L = 0.8 is 1.28 dB. When Ma = 3.0, 3.5 and 4.0, the *SPL* within the cavity under the control of *Sawtooth* 1–3 are obviously higher than that at the basic state, so the leading edge sawtooth could no longer suppress the cavity noise. Therefore, when the Ma increases to certain critical value between 2.5~3.0, leading edge sawtooth of the three parameters would completely lose their suppression effect on cavity noise and increase the noise. When the total height of the sawtooth remains constant, variations in the sawtooth height have minimal impact on the sound pressure level within the cavity. However, when the height of the sawtooth base is fixed, changes in the sawtooth height exert significant influence on the sound pressure level in the cavity. Specifically, as the sawtooth height decreases, there is a corresponding reduction in the sound pressure level within the cavity.
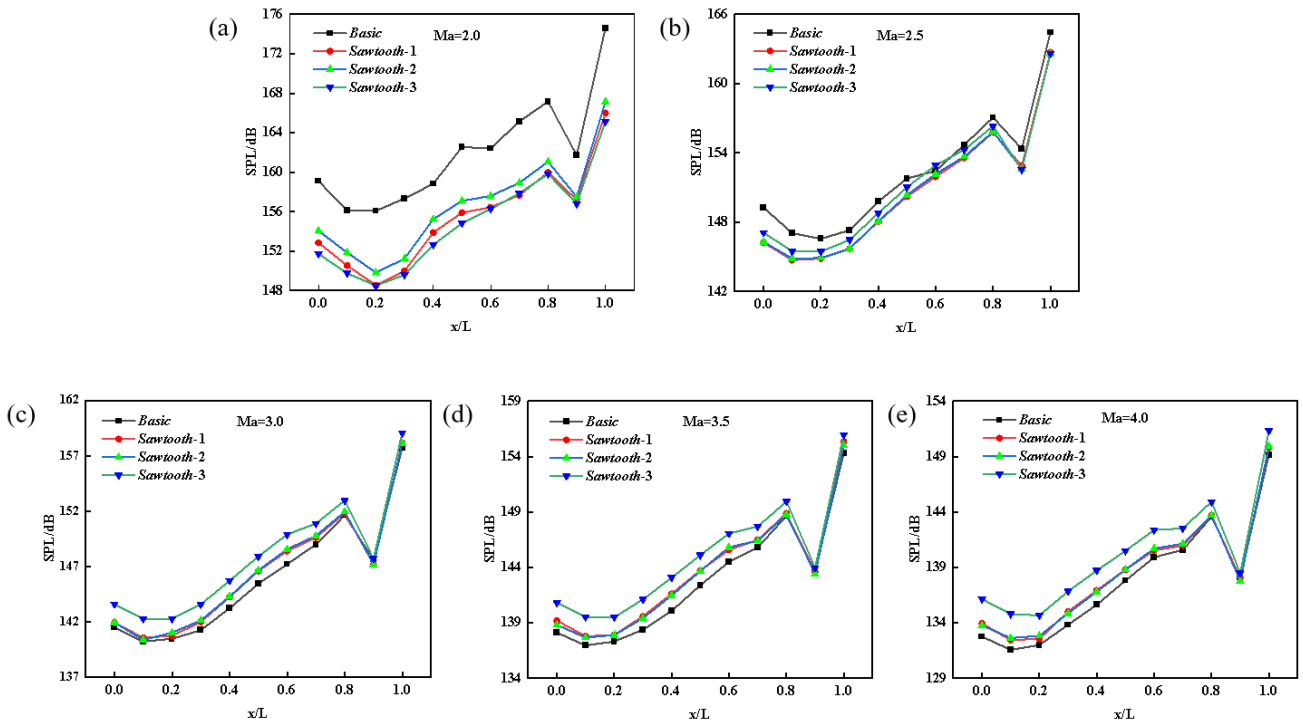

Figure 5. *SPL* distribution of measuring points within the cavity under leading edge sawtooth control: **(a)** Ma = 2.0; **(b)** Ma = 2.5; **(c)** Ma = 3.0; **(d)** Ma = 3.5; **(e)** Ma = 4.0.

To study the *SPFS* performance of cavity acoustic load under leading edge sawtooth control, the *SPFS* of fluctuating pressure under the control of *Sawtooth*-1 was analyzed (**Figure 6**). The abscissa is the discrete frequency of the noise test data and the ordinate is the corresponding noise *SPFS* of various frequencies. It can be seen that, at the cavity $x/L = 0.8$, when Ma = 2.0, the *SPFS* amplitude of fluctuating pressure is 135.44 dB at the peak frequency of 1379.40 Hz; when Ma = 2.5, the *SPFS* amplitude of fluctuating pressure is 122.78 dB at the peak frequency of 268.55 Hz; when Ma = 3.0, the *SPFS* amplitude of fluctuating pressure is 117.92 dB at the peak frequency of 286.87 Hz; when Ma = 3.5, the *SPFS* amplitude of fluctuating pressure is 114.81 dB at the peak frequency of 286.87 Hz; when Ma = 4.0, the *SPFS* amplitude of fluctuating pressure is 109.50 dB at the peak frequency of 305.18 Hz. The maximum *SPFS* of fluctuating pressure appears in the low frequency region and it gradually decreases with the gradual increase of Ma.
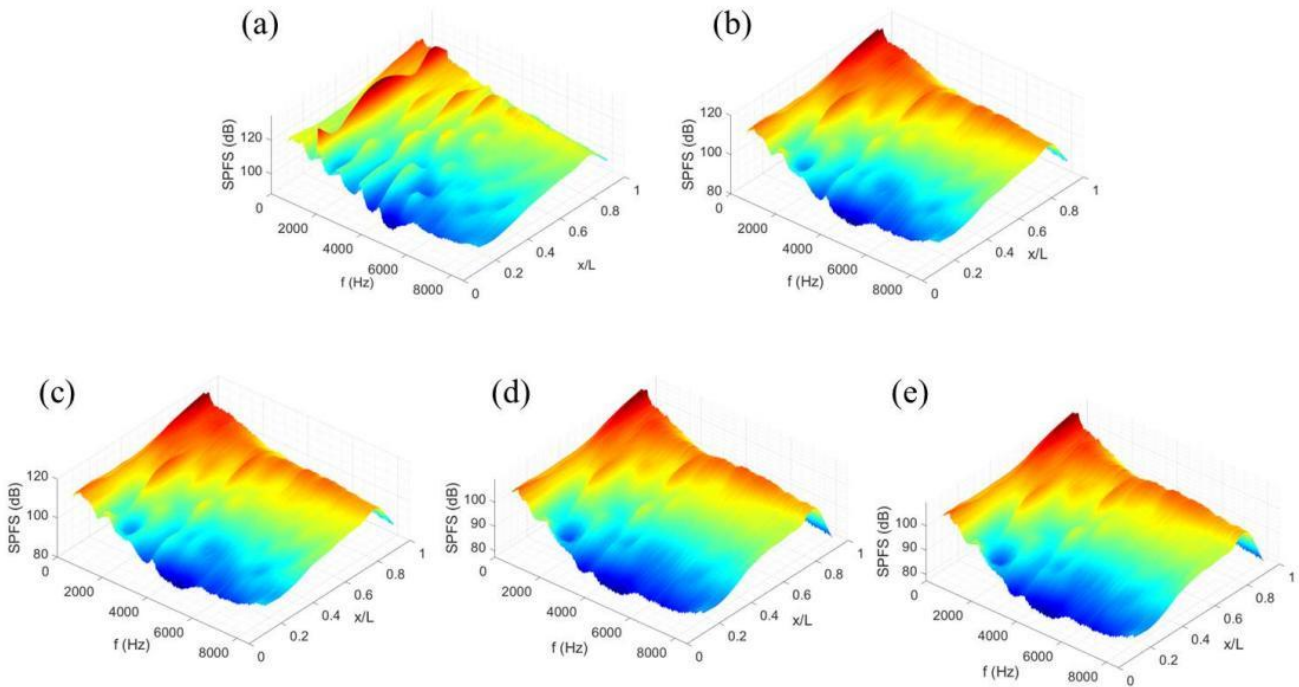

Figure 6. *SPFS* distribution within the cavity under the control of *Sawtooth*-1: **(a)** Ma = 2.0; **(b)** Ma = 2.5; **(c)** Ma = 3.0; **(d)** Ma = 3.5; **(e)** Ma = 4.0.

It can be seen from **Figure 6** that the *SPFS* at the cavity $x/L > 0.5$ is strong and the suppression effect of *Sawtooth*-1 towards that region is evident. Therefore, the characteristics of cavity noise are further analyzed based on the *SPFS* at the cavity $x/L = 0.8$. The *SPFS* at the cavity $x/L = 0.8$ under basic state and *Sawtooth*-1 control are compared in **Figure 7**. When Ma = 2.0~4.0, the peak values of *SPFS* at basic state and *Sawtooth*-1 control remain the same, which demonstrates that the leading edge sawtooth basically has no effect on the modal frequency of cavity noise. When Ma = 2.0 and 2.5, the *SPFS* curves within cavity installed with *Sawtooth*-1 translates downward obviously, and the broadband noise and peak noise are influenced; while when Ma = 3.0, 3.5 and 4.0, the *SPFS* curves at basic state and *Sawtooth*-1 control state are basically the same.
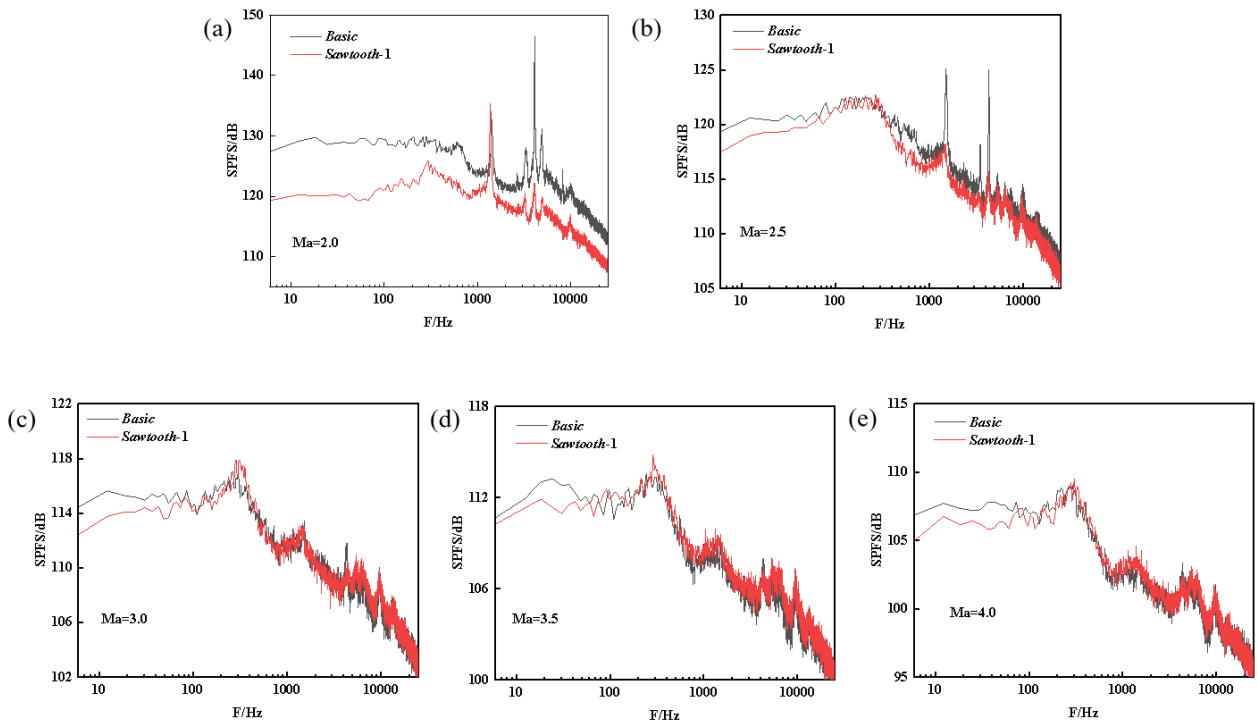
Figure 7. *SPFS* of measuring point at the cavity *x/L* = 0.8 under the control of *Sawtooth*-1: **(a)** Ma = 2.0; **(b)** Ma = 2.5; **(c)** Ma = 3.0; **(d)** Ma = 3.5; **(e)** Ma = 4.0.

3.3. Suppression effect of leading edge cylinder on high-speed cavity noise

By comparing the *SPL* distribution curves on the centerline of the inner wall of the cavity under leading edge cylinder control of various dimension parameters, the influence of leading edge cylinder on cavity noise could be analyzed. Concrete dimensions of the leading edge cylinder are shown in **Figure 8**.
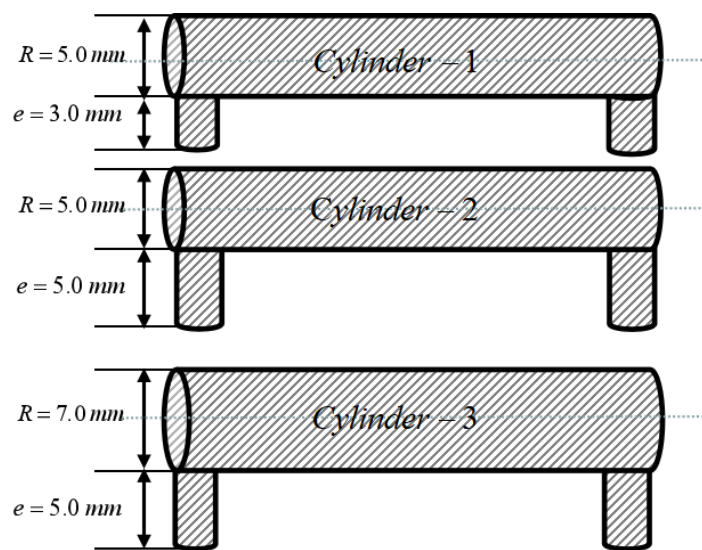

Figure 8. Leading edge cylinder of various parameters.

The *SPL* distribution of various measuring points within the cavity under leading edge cylinder of various parameters in all Mach numbers is shown in **Figure 9**. It can

be observed that the test results are similar to those under leading edge sawtooth. In the cavity $x/L < 0.5$ region, along with the streamwise position of the centerline within the cavity, the *SPL* shows a declining trend, followed by a increasing one, and the *SPL* within the cavity is the smallest in the cavity $x/L = 0.1$. In the cavity $x/L > 0.5$ region, the *SPL* shows an increasing-decreasing-increasing trend of along with the streamwise position of the centerline within the cavity, and the maximum *SPL* within the cavity appears at the $x/L = 1.0$ at the aft wall of the cavity. By observing the *SPL* curves in **Figure 9** that, it can be seen that when Ma = 2.0 and 2.5, the *SPL* within the cavity declines with the increase of leading edge cylinder *e* under the condition of same leading edge cylinder R; and the *SPL* within the cavity changes slightly with the increase of leading edge cylinder R under the condition of same leading edge cylinder *e*. Considering the influence of control conditions on the aerodynamic performance and flight performance of craft, the comprehensive performance of *Cylinder*-2 is better than others. When Ma = 2.0 and 2.5, the decrease of *SPL* at the cavity $x/L = 0.8$ under the control of *Sawtooth*-1 reaches 8.08 dB and 0.84 dB, respectively. When Ma = 3.0, 3.5 and 4.0, the *SPL* within the cavity under the control of *Cylinder* 1–3 is obviously higher than that at the basic state. Similar to leading edge sawtooth control, after the Ma increases to certain critical value between 2.5~3.0, leading edge cylinder of the three parameters would completely lose their suppression effect on cavity noise and increase the noise. When the diameter of the leading edge cylinder remains constant, the height of the cylinder has a significant impact on the sound pressure level within the cavity. Specifically, as the cylinder height increases, the sound pressure level in the cavity decreases. Conversely, when the cylinder height is kept constant, the variation in cylinder diameter has a minimal effect on the sound pressure level. However, the sound pressure level does decrease with an increase in cylinder diameter at Mach numbers of 3.0, 3.5, and 4.0.
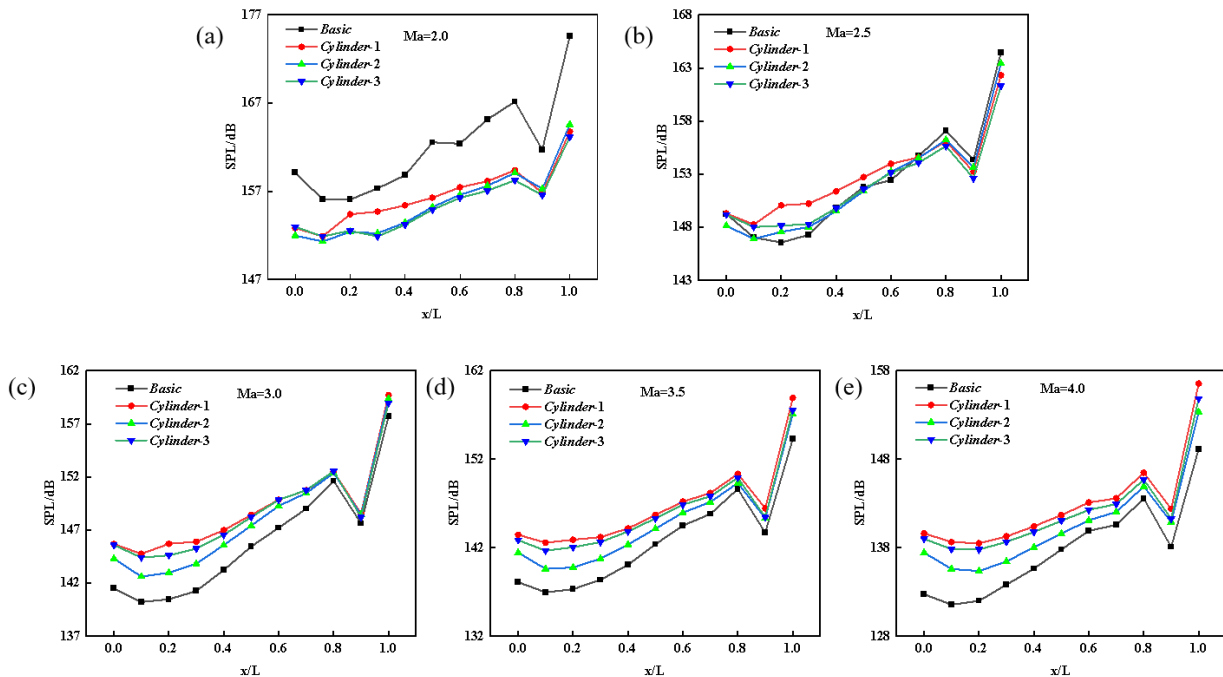

Figure 9. *SPL* distribution of measuring points within the cavity under leading edge cylinder control: **(a)** Ma = 2.0; **(b)** Ma = 2.5; **(c)** Ma = 3.0; **(d)** Ma = 3.5; **(e)** Ma = 4.0.

To study the *SPFS* performance of cavity acoustic load under leading edge cylinder control, the *SPFS* of fluctuating pressure under the control of *Cylinder*-2 is analyzed in **Figure 10**. It can be seen that, at the cavity *x/L* = 0.8, when Ma = 2.0, 2.5, 3.0, 3.5 and 4.0, the *SPFS* amplitudes of fluctuating pressure are 125.39 dB, 123.40 dB, 119.31 dB, 117.34 dB and 112.09 dB at the peak frequency of 205.24 Hz, 207.52 Hz, 164.79 Hz, 140.38 Hz and 170.90 Hz, respectively. The maximum *SPFS* of fluctuating pressure appears in the low frequency region and gradually decreases with the gradual increase of Ma.
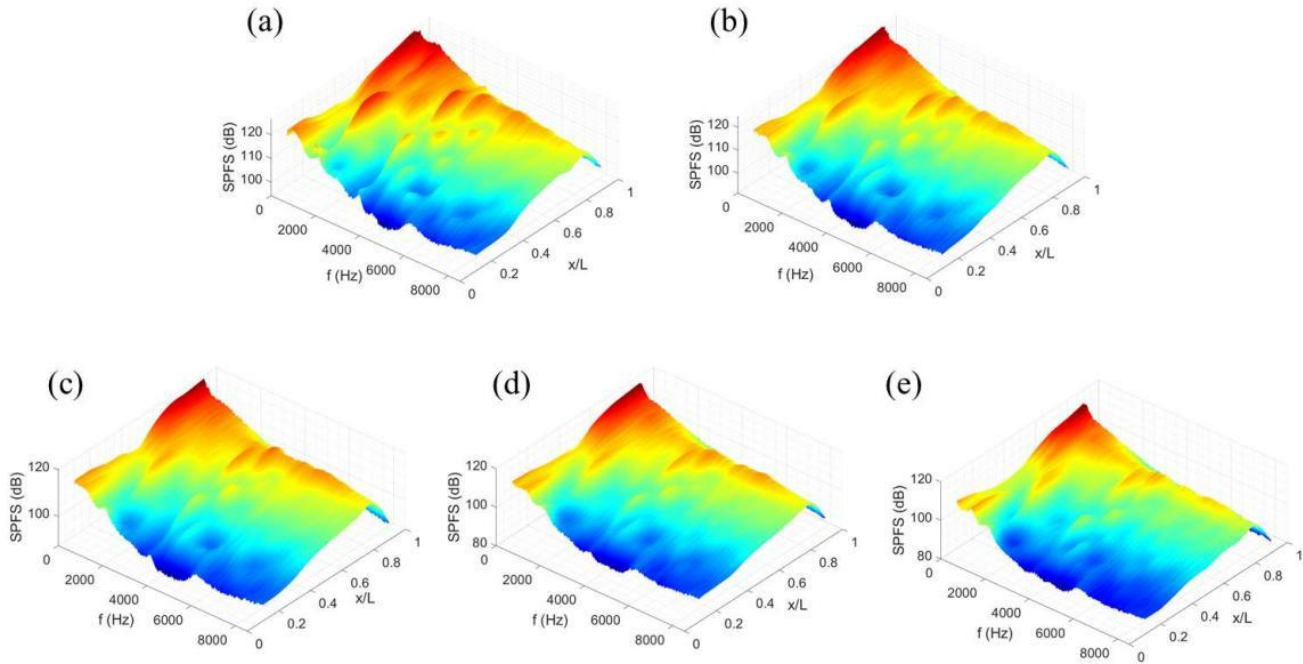

Figure 10. *SPFS* distribution within the cavity under the control of *Cylinder*-2: **(a)** Ma = 2.0; **(b)** Ma = 2.5; **(c)** Ma = 3.0; **(d)** Ma = 3.5; **(e)** Ma = 4.0.

It can be observed from **Figure 10** that the *SPFS* at the cavity *x/L* > 0.5 is stronger and the suppression effect of *Cylinder*-2 towards the region is evident. Therefore, the characteristics of cavity noise are further analyzed based on the *SPFS* at the cavity *x/L* = 0.8. The *SPFS* at the cavity *x/L* = 0.8 under basic state and *Cylinder*-2 control are compared in **Figure 11**. When Ma = 2.0~4.0, the peak values of *SPFS* at basic state and *Cylinder*-2 control remain the same, indicating that the leading edge sawtooth basically has no effect on the modal frequency of cavity noise. When Ma = 2.0 and 2.5, the *SPFS* curves within cavity installed with *Cylinder*-2 significantly translates downward, and the broadband noise and peak noise are influenced; while when Ma = 3.0, 3.5 and 4.0, the *SPFS* curves within cavity installed with *Cylinder*-2 are higher than those at basic state.
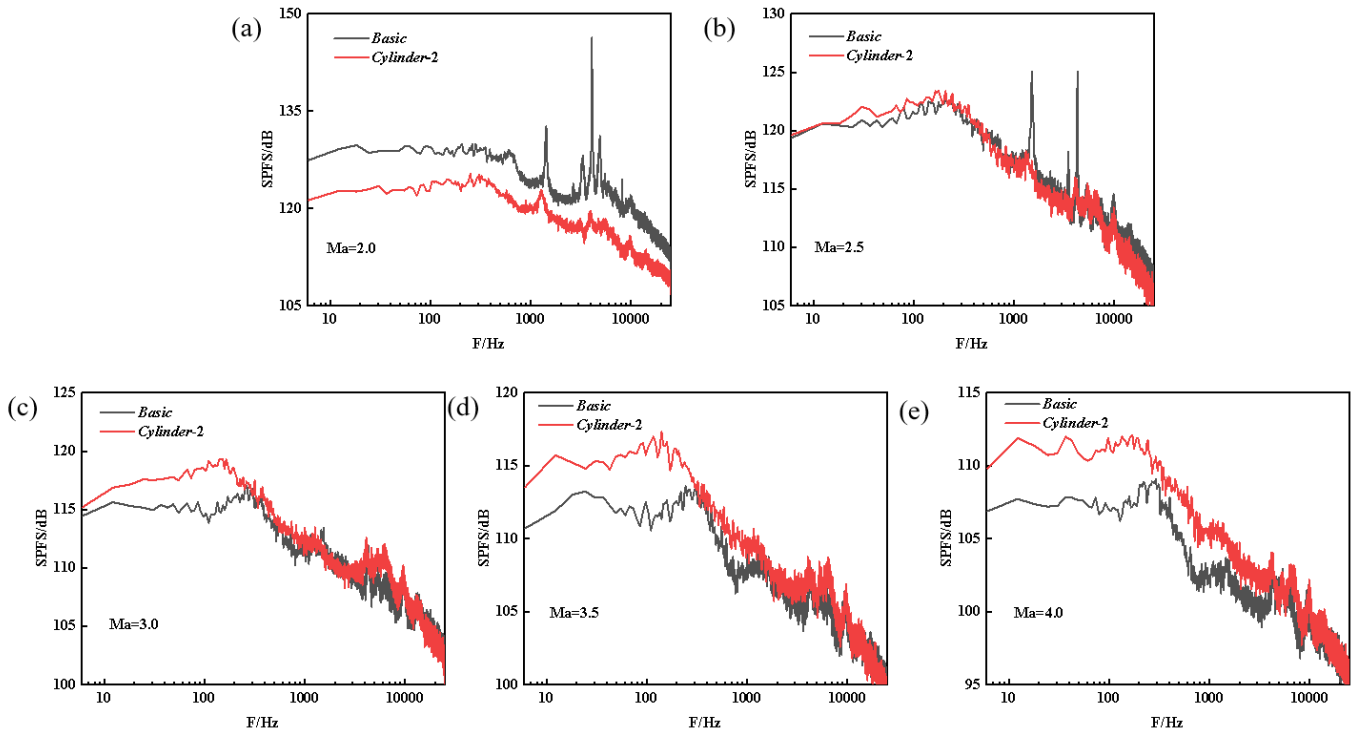
Figure 11. *SPFS* of measuring points at cavity *x/L* = 0.8 under the control of *Cylinder*-2: **(a)** Ma = 2.0; **(b)** Ma = 2.5; **(c)** Ma = 3.0; **(d)** Ma = 3.5; **(e)** Ma = 4.0.

3.4. Suppression effect of trailing edge contouring on high-speed cavity noise

The dimension parameters of trailing edge contouring are shown in **Figure 2c** and the tilt angles of trailing edge are 90° chamfer, 120° and 135°, respectively. The influence of trailing edge contouring on cavity noise is analyzed by comparing the *SPL* distribution curves on the inner wall centerline under trailing edge contouring control of various dimension parameters, as shown in **Figure 12**. The *SPL* within the cavity of trailing edge contouring is lower than that at basic state and it declines with the increase of Ma. When Ma = 2.0 and 2.5, the *SPL* within the cavity under the control of trailing edge $\theta = 90°$ chamfer is higher than the others; when Ma = 3.0, 3.5 and 4.0, the suppression effect of the three trailing edge contouring on cavity noise is similar, and the suppression effect gradually decreased with the increase of Ma. The suppression effect of trailing edge contouring $\theta = 120°$ is the best. When Ma = 2.0~4.0, the decrease of *SPL* at the cavity *x/L* = 0.8 under the control of trailing edge contouring $\theta = 120°$ reaches 1.92 dB, 1.86 dB, 1.23 dB, 1.63 dB and 1.04 dB, respectively. High-speed air flows are separated at the smooth plate at the front end of the model, and part of the air flows into the cavity and expands, resulting in a slight reduction of SPL at the leading edge of the inner wall of the cavity. In comparison, the other part flows downstream to form a shear layer above the cavity, which crosses the middle of the cavity and collides with the rear wall. As the angle of the back wall increases, the vertical collision between the shear layer and the back wall of the cavity changes to the inclined collision. The component of sound pressure generated by collision on the normal of the back wall of the cavity is weakened, so the *SPL* near the back wall of the cavity is reduced. In addition, due to the increase of the angle of the back wall of

the cavity, the collision between the shear layer and the back wall of the cavity is weakened, resulting in the weakening of the pulsating pressure intensity within the cavity and the decrease of the *SPL* within the cavity [36,37].
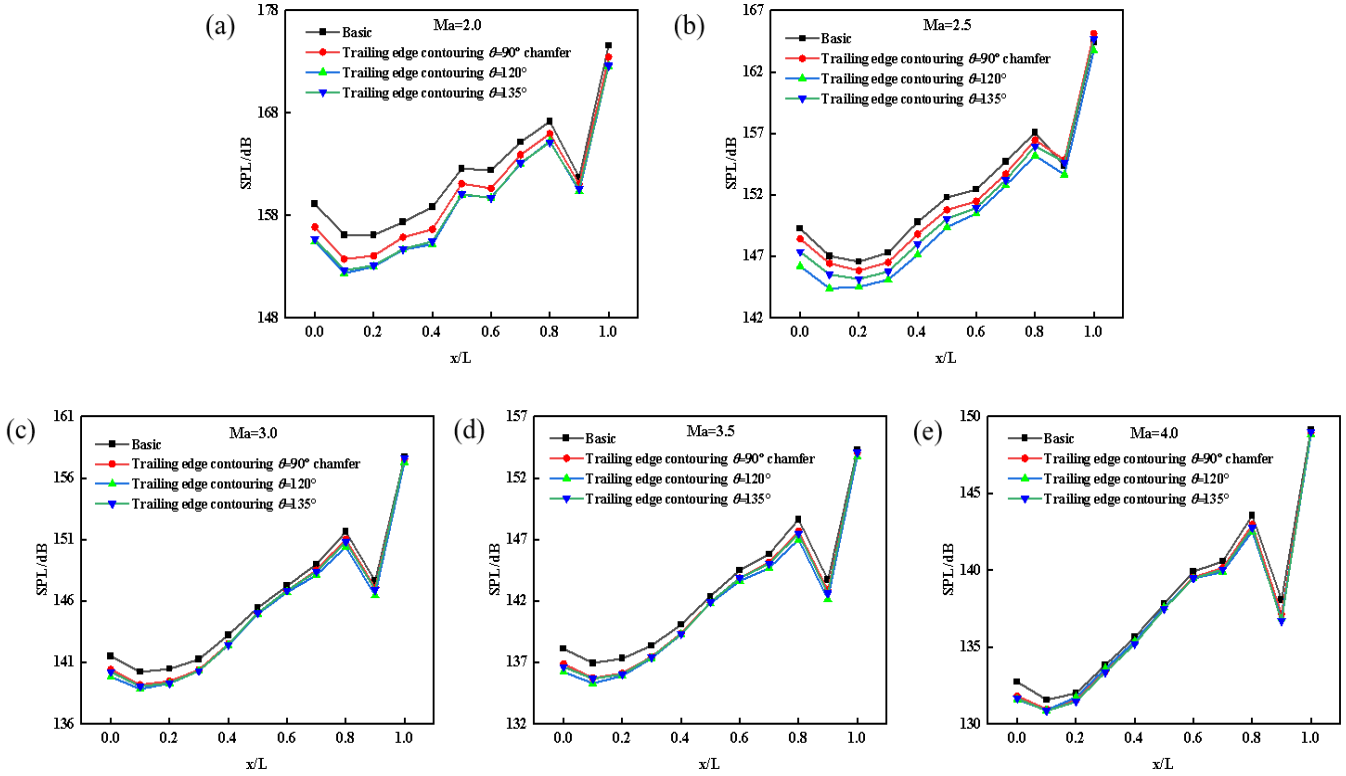

Figure 12. *SPL* distribution of measuring points within the cavity under trailing edge contouring control: **(a)** Ma = 2.0; **(b)** Ma = 2.5; **(c)** Ma = 3.0; **(d)** Ma = 3.5; **(e)** Ma = 4.0.

To study the *SPFS* performance of cavity acoustic load under trailing edge contouring control, the *SPFS* of fluctuating pressure under the control of trailing edge contouring $\theta = 120°$ is analyzed in **Figure 13**. At the cavity $x/L = 0.8$, when Ma = 2.0, the *SPFS* amplitude of fluctuating pressure is 147.00 dB at the peak frequency of 4077.10 Hz; when Ma = 2.5, the *SPFS* amplitude of fluctuating pressure is 122.76 dB at the peak frequency of 231.93 Hz; when Ma = 3.0, the *SPFS* amplitude of fluctuating pressure is 116.46 dB at the peak frequency of 244.14 Hz; when Ma = 3.5, the *SPFS* amplitude of fluctuating pressure is 112.53 dB at the peak frequency of 292.97 Hz; when Ma = 4.0, the *SPFS* amplitude of fluctuating pressure is 107.4 dB at the peak frequency of 244.14 Hz. The maximum *SPFS* of fluctuating pressure appears in the low frequency region and it gradually decreases with the gradual increase of Ma.

It can be observed from **Figure 13** that the *SPFS* at the cavity $x/L > 0.5$ is strong and the suppression effect of trailing edge contouring $\theta = 120°$ towards the region is evident. Therefore, the characteristics of cavity noise are further analyzed based on the *SPFS* at the cavity $x/L = 0.8$. The *SPFS* at the cavity $x/L = 0.8$ under basic state and trailing edge contouring $\theta = 120°$ control are compared in **Figure 14**. When Ma = 2.0~4.0, the peak values of *SPFS* at basic state and trailing edge contouring $\theta = 120°$ control remain the same, showing that the leading edge sawtooth basically has no effect on the modal frequency of cavity noise. When Ma = 2.0 and 2.5, the *SPFS* curves within cavity installed with *Sawtooth*-1 translates downward obviously. The

broadband noise and peak noise are influenced obviously, but the suppression effect gradually decreases with the increase of frequency.
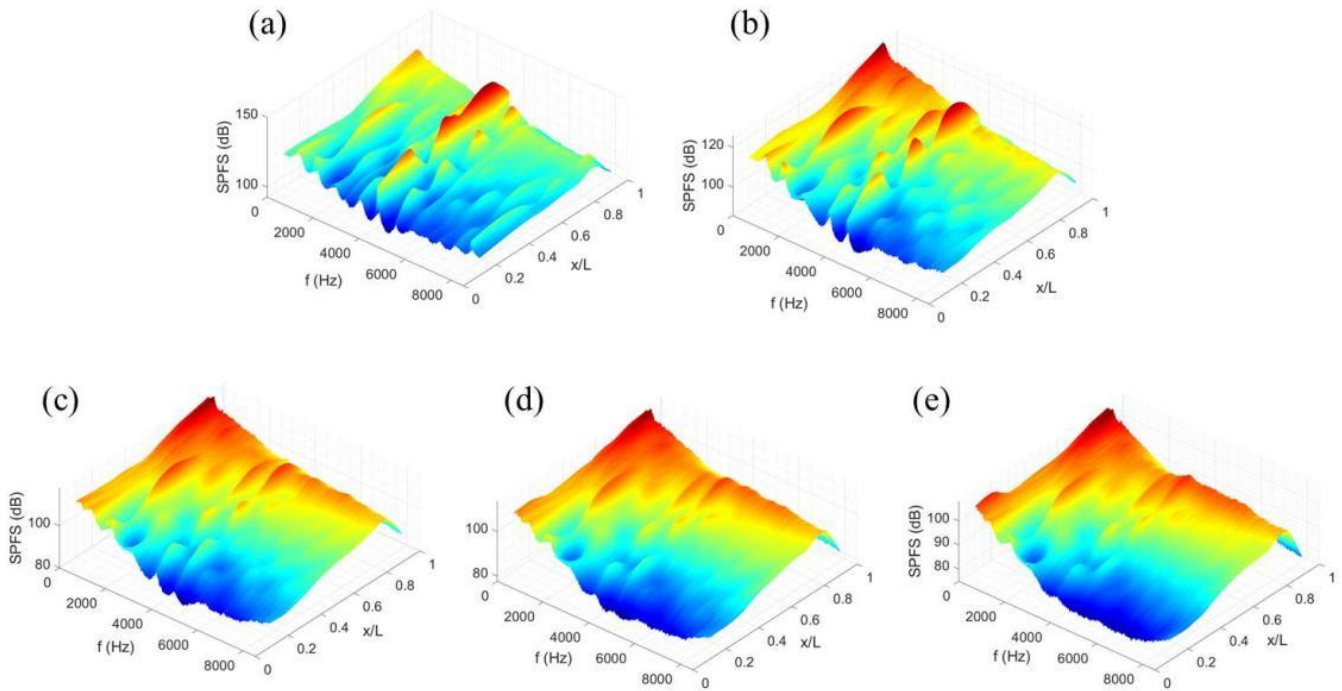

Figure 13. *SPFS* distribution within the cavity under the control of trailing edge contouring $\theta = 120°$: **(a)** Ma = 2.0; **(b)** Ma = 2.5; **(c)** Ma = 3.0; **(d)** Ma = 3.5; **(e)** Ma = 4.0.

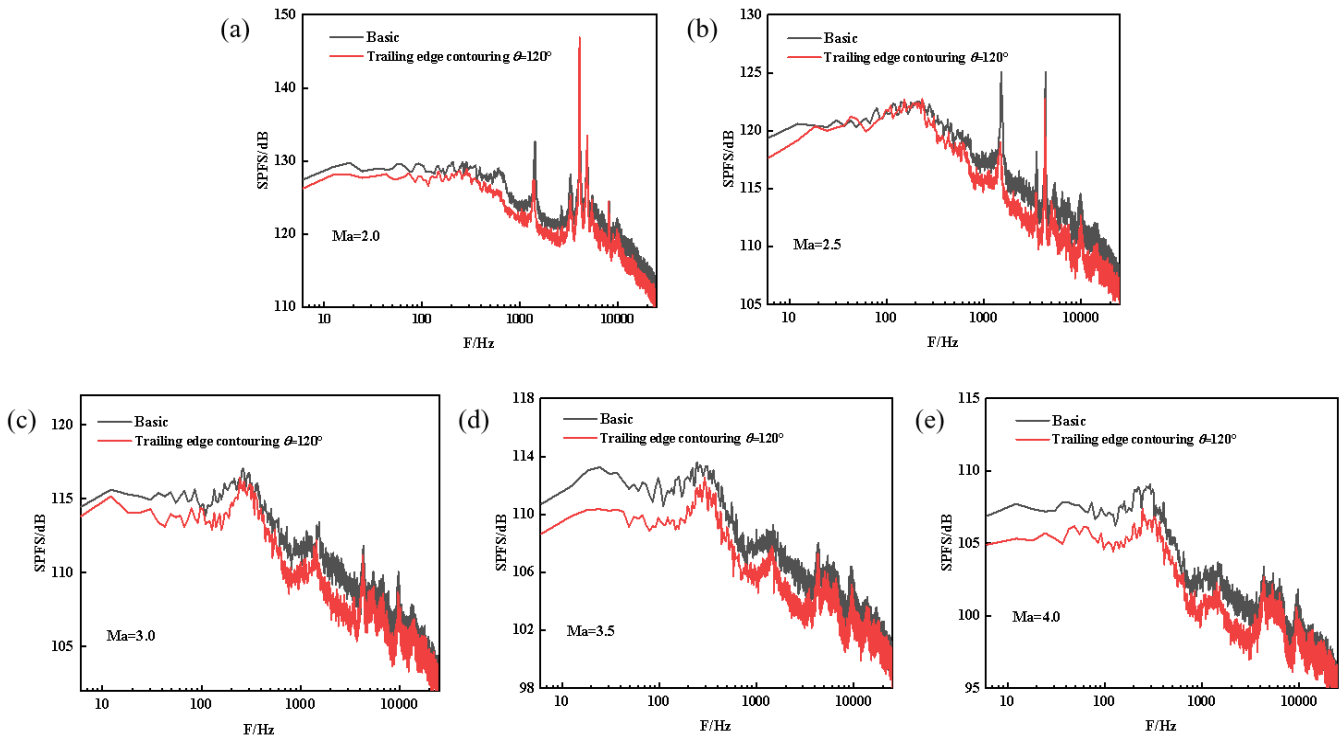**Figure 14.** *SPFS* of measuring points at the cavity $x/L = 0.8$ under the control of trailing edge contouring $\theta = 120°$: **(a)** Ma = 2.0; **(b)** Ma = 2.5; **(c)** Ma = 3.0; **(d)** Ma = 3.5; **(e)** Ma = 4.0.

4. Conclusion

This study explored the suppression effect of leading edge sawtooth, cylinder and trailing edge contouring on C201 standard cavity noise under the condition of supersonic flow by high-speed wind tunnel test. By analyzing the *SPL* and *SPFS* distribution within the cavity under the control of leading edge sawtooth, cylinder and trailing edge contouring with different parameters, the control conditions are optimized. When Ma = 2.0 and 2.5, the decrease of *SPL* at the cavity $x/L = 0.8$ reaches 7.18 dB and 1.28 dB, respectively, under the control of *Sawtooth*-1 ($H = 7.73$ mm, $h^* = 6.00$ mm, $h = 6.00$ mm); the decrease of *SPL* at the cavity $x/L = 0.8$ reach 8.08 dB and 0.84 dB, respectively, under the control of *Cylinder*-2 ($R = 5.0$ mm, $e = 5.0$ mm). While when Ma = 3.0, 3.5 and 4.0, the leading edge sawtooth and cylinder could no longer suppress cavity noise. Therefore, after the Ma increases to certain critical value between 2.5~3.0, leading edge sawtooth and cylinder would completely lose their suppression effect on cavity noise and the noise is increased. When Ma = 2.0~4.0, the decrease of *SPL* at the cavity $x/L = 0.8$ under the control of trailing edge contouring $\theta = 120°$ reach 1.92 dB, 1.86 dB, 1.23 dB, 1.63 dB and 1.04 dB, respectively. Different from the leading edge sawtooth and cylinder, although the suppression effect of trailing edge contouring on the cavity noise at supersonic conditions gradually decreases with the increase of Ma, it has a certain suppression effect when Ma = 2.0~4.0.

Conflict of interest: The authors declare no conflict of interest.

References

1. Shaw L, Clark R, Talmadge D. F-111 generic weapons bay acoustic environment. Journal of Aircraft, 1988, 25(2): 147–153.
2. Zhao K, Okolo P, Neri E, et al. Noise reduction technologies for aircraft landing gear-A bibliographic review. Pergamon, 2020.
3. Flaherty W, Reedy T, Elliott G S, et al. Investigation of cavity flow using fast-response pressure-sensitive paint. AIAA Journal, 2014, 52 (11): 2462–2470.

4. Shaaban M, Mohany A. Passive control of flow-excited acoustic resonance in rectangular cavities using upstream mounted blocks. Experiments in Fluids, 2015, 56: 1–12.

5. Stanek M, Raman G, Ross J, et al. High frequency acoustic suppression-the role of mass flow & the notion of superposition. AIAA Aeroacoustics Conference. 2002: 2404.

6. Schmit R, Semmelmayer F, Haverkamp M, et al. Analysis of cavity passive flow control using high speed shadowgraph images. AIAA Aerospace Sciences Meeting Including the New Horizons Forum and Aerospace Exposition. 2012: 738.

7. Schmit R, Semmelmayer F, Haverkamp M, et al. Examining passive flow control devices with high speed shadowgraph images around a Mach1. 5 cavity flow field. AIAA Flow Control Conference. 2012: 3139.

8. Thangamani V, Knowles K, Saddington A J. Effects of scaling on high subsonic cavity flow oscillations and control. Journal of Aircraft, 2014, 51 (2): 424–433.

9. Saddington A J, Knowles K, Thangamani V. Scale effects on the performance of sawtooth spoilers in transonic rectangular cavity flow. Experiments in Fluids, 2016, 57: 1–12.

10. Panickar P, Raman G. Understanding the mechanism of cavity resonance suppression using a cylindrical rod in crossflow. AIAA Aerospace Sciences Meeting and Exhibit. 2008: 54.

11. Dudley J, Ukeiley L. Suppression of fluctuating surface pressures in a supersonic cavity flow. Flow Control Conference. 2010: 4974.

12. Dudley J G, Ukeiley L. Passively controlled supersonic cavity flow using a spanwise cylinder. Experiments in Fluids, 2014, 55: 1–22.

13. Dangguo Y, Jifei W. Investigation on suppression effect of zero-net-mass-flux jet on aerodynamic noise inside open cavities. Acta Aeronautica Et Astronautica Sinica, 2011, 32(6): 1007–1014.

14. Ananthan V B, Akkermans R A D, Hu T, et al. Effect of porous material on trailing edge sound sources of a lifting airfoil by zonal Overset-LES. Journal of Sound and Vibration, 2020, 480 (10): 115386.

15. Ananthan V B, Akkermans R A D, Hu T, et al. Trailing-edge noise reduction potential of a locally applied shallow dimpled surface. Journal of Sound and Vibration, 2022, 525: 116745.

16. Ananthan V B, Akkermans R A D, Hu T, et al. Effects of localized application of porous material on trailing-edge noise of a circulation-controlled wing. International Journal of Heat and Fluid Flow, 2023, 103: 109209.

17. Ananthan V B, Akkermans R A D, Hu T, et al. Trailing edge noise reduction using bio-inspired finlets. Journal of Sound and Vibration, 2023, 549: 117553.

18. Kähler H H, Bliss D B. Aerodynamically induced pressure oscillations in cavities-physical mechanisms and suppression concepts. 1975.

19. Plumblee H E, Gibson J S, Lassiter L W. A theoretical and experimental investigation of the acoustic response of cavities in an aerodynamic flow. 1962.

20. Hankey W L, Shang J S. Analyses of pressure oscillations in an open cavity. AIAA Journal, 2012, 18 (8): 892–898.

21. Sun X H, Zhang P J Y, Zhao K, et al. Effects of Mach number on space-time characteristics of wall pressure fluctuations beneath turbulent boundary layers. Physics of Fluids, 2024, 36(9).

22. Yu M, Dong S W, Liu P X, et al. Post-shock turbulence recovery in oblique-shock/turbulent boundary layer interaction flows. Journal of Fluid Mechanics, 2023, 961: A26.

23. Abdelmwgoud M, Shaaban M, Mohany A. Shear layer synchronization of aerodynamically isolated opposite cavities due to acoustic resonance excitation. Physics of Fluids, 2021, 33(5).

24. Karthick S K. Shock and shear layer interactions in a confined supersonic cavity flow. Physics of Fluids, 2021, 33(6).

25. Sah R, Ghosh S. Numerical Investigation of Supersonic Turbulent Flow Over Open Cavities. International Journal of Fluid Mechanics & Thermal Sciences, 2021, 7(2): 22–31.

26. Chen B, Wang Y. Active aerodynamic noise control research for supersonic aircraft cavity by nonlinear numerical simulation. International Journal of Electrical Engineering & Education, 2023, 60: 2397–2411.

27. Song W, Ai B, Zhao X, et al. Influence of control device on store separation from an open cavity. Aerospace Science and Technology, 2020, 106: 106117.

28. Kong Y, Wu Y, Zong H, et al. Supersonic cavity shear layer control using spanwise pulsed spark discharge array. Physics of Fluids, 2022, 34(5).

29. Dangguo Y, Jun L, Xiansheng W, et al. Analysis of design method and aeroacoustics characteristics inside typical cavity. Acta Aerodynamica Sinica, 2018, 36(3): 432–439.

30. Xiansheng W, Dangguo Y, Fangqi Z, et al. Suppression of the cavity oscillation using high-speed mass injection. International Journal of Modern Physics B, 2020, 34: 2040098.

31. Xiansheng W, Dangguo Y, Jun L, et al. Control of pressure oscillations induced by supersonic cavity flow. AIAA Journal, 2020, 58 (5): 2070–2077.

32. Qinghe Z, Shuyang F, Fangqi Z, et al. Experimental investigation of passive control for cavity noise in high-speed flow using sawtooth spoiler. Applied Acoustics, 2023, 211: 109567.

33. Jun L, Jisheng C, Dangguo Y, et al. Research progress in wave evolution and noise control for supersonic cavity flows. Hangkong Xuebao/Acta Aeronautica Et Astronautica Sinica, 2018, 39(11): 022366.

34. Hall A, Atassi O, Gilson J, et al. Effect of leading-edge thickness on high-speed airfoil-turbulence interaction noise. AIAA/CEAS Aeroacoustics Conference. 2011.

35. Bross M, Scharnowski S, Kähler C J. Influence of leading edge tripping devices on supersonic turbulent boundary layer characteristics. The 5th International Conference on Experimental Fluid Mechanics, ICEFM 2018 Munich. 2018.

36. Wu J, Xu L, Fan Z, et al. Effect of chamfer rear-face angle on open cavity flow aero-acoustic noise suppression. Acta Aerodynamica Sinica, 2017, 35 (5): 645–649.

37. Yuan S K, Li R N. Analysis Influence of Trailing Edge Modification on Aerodynamic Performance of Airfoils for Wind Turbine. Applied Mechanics and Materials, 2012, 220–223: 900–904.